

# MULTIAXIAL FATIGUE BEHAVIOUR OF A SHORT-FIBRE REINFORCED POLYAMIDE 6.6 IN THE PRESENCE OF NOTCHES

M. De Monte<sup>1</sup>, E. Moosbrugger<sup>1</sup>, M. Quaresimin<sup>2</sup>

<sup>1</sup> Corporate Sector Research and Advance Engineering - Advance Production Technology 1 – Plastics Engineering (CR/APP2), Robert Bosch GmbH, Postbox 1131, 71301 Waiblingen (Germany)

<sup>2</sup> Department of Management and Engineering, University of Padova, Stradella S. Nicola 3, 36100 Vicenza (Italy)

## ABSTRACT

This paper deals with the multiaxial fatigue behaviour of notched hollow tubular specimens made of a short fibre reinforced polyamide 6.6 (PA66-GF35). Fatigue tests were carried out at room temperature under a combination of tensile and torsional loading, considering the influence of load ratio and biaxiality ratio. The investigations represent an extension of the multiaxial fatigue characterisation on plain hollow specimens previously carried out by the authors.

The fatigue curves on notched specimens are compared to the relevant test series on plain hollow specimens, revealing pronounced notch sensitivity under axial loading, whereas no strength reduction is observed under torsional loading. A further torsional test series on a specimen containing a drilled hole suggests that the apparent notch insensitivity is actually the result of compensation between the stress contraction introduced by the notch and effects induced by local morphology and failure modes.

## 1. INTRODUCTION

Injection moulded short-fibre reinforced thermoplastic components (SF RTP) present often very complex shapes, with transition radii, thickness variations and holes. The fatigue strength assessment of such components requires a comprehensive investigation of the notch effect on fatigue strength, under uniaxial as well as multiaxial loading conditions. In order to reduce testing efforts on components and develop a fatigue failure assessment method of general applicability, it is necessary to evaluate the material characteristic values under cyclic loading on standard specimens and to develop a FEA-based methodology to transfer them to real components.

Few investigations on the multiaxial fatigue behaviour of composites in the presence of notches can be found in literature. Among them, Francis *et al.* [1] carried out biaxial fatigue tests on thin-walled tubular specimens (diameter: 25.4 mm), made of graphite/epoxy composite with different fibre lay-ups, containing a 4.8 mm diameter hole. For the [0/90]<sub>s</sub> tubes, they found extensive transverse cracking under pure torsional loading, while clean fracture perpendicular to the 0° plies was noticed under pure axial loading. Fujii *et al.* [2] investigated the fatigue notch sensitivity of woven fabric composites on thin-walled tubular specimens containing a drilled hole under tension-torsion loading. They report almost no notch sensitivity under shear stress for this material.

The influence of notches on fatigue strength of PA66-GF35 under uniaxial loading has been already analysed in a previous investigation [3], using rectangular cross-section specimens. A strain energy density (SED) method to account for the notch-effect, based on local averaged SED over a control volume, has been proposed in [4]. For thick specimens under an external uniaxial loading, the presence of notches induces a multiaxial stress state around the notch tip: a geometrical multiaxiality is introduced. The multiaxial fatigue behaviour of PA66-GF35 has been already investigated on

tubular hollow specimens in a previous work [5]. In this paper the characterization will be extended to notched specimens, comparing the resulting fatigue curves to the relevant ones obtained on plain specimens.

## 2. EXPERIMENTAL PROGRAM

The material investigated in this work is a short fibre reinforced polyamide 6.6, containing 35% wt. glass fibres (designation PA66-GF35). Fibres have a nominal diameter of 10  $\mu\text{m}$  and an average fibre length, after injection moulding, in the range 240÷280  $\mu\text{m}$ . The glass transition temperature  $T_g$  of the dry material is 65°C.

Hollow tubular samples containing a sharp V-notch have been obtained by injection moulding through a ring gate; the specimen and notch geometry are reported in Figure 1. In the central part fibres are mainly oriented along the axis of the tubular specimen (X direction in Figure 1).

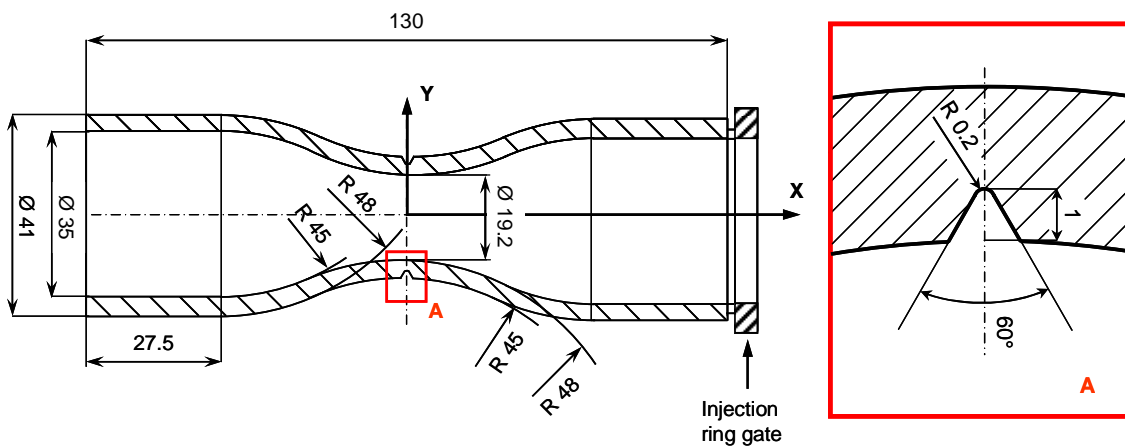


**Figure 1:** V-notched specimen geometry (a) with detail of the notch (b). Dimensions in mm

Fatigue tests were carried out on dry as moulded specimens (relative humidity RH under 0.1 %) at different load ratios R (R=0 and R=-1) and temperatures (RT and 130°C), with constant load amplitude and frequency.

The following experimental program has been carried out on an axial-torsional servo-hydraulic machine at the Fraunhofer Institute for Structural Durability and System Reliability LBF, Darmstadt (Germany):

- two series of tests under pure tensile loading (R=0 and R=-1 at RT)
- two series of tests under pure torsional loading (R=0 and R=-1 at RT)
- two series of tests under combined in-phase tensile-torsional loading (R=0 and R=-1 at RT) with biaxiality ratio  $\lambda_2 = 1$ ,  $\delta = 0^\circ$
- one series of tests under combined in-phase tensile-torsional loading (R=0) at RT with biaxiality ratio  $\lambda_2 = 1/3$ ,  $\delta = 0^\circ$

where  $\lambda_2 = \tau_{12,a} / \sigma_{1,a}$  is the shear biaxiality ratio on nominal net stress amplitudes in the material coordinate system and  $\delta$  is the phase-shifting angle between the tensile and torsional load components. The load frequencies were chosen so that the temperature measured on specimen surface did not exceed the test temperature of more than 5°C. In order to increase the test frequencies an air-cooling system was adopted, blowing air on both the external and internal specimen surfaces. The deriving frequencies were between 1 and 6 Hz, resulting in a testing time for each sample between 0.5 hours and



**Figure 2:** Servo-hydraulic testing machine used to test the V-notched specimens

10 days. The loading wave was sinusoidal and the tests were performed under load and torque control. The testing system (Figure 2) can generate and control the axial and the torsion loads independently from each other. Under pure cyclic torsion, the specimen was free to move in axial direction, allowing the necessary axial displacements to keep the axial load to zero. The adopted clamping system has been described in [5]. The general criterion for ending fatigue tests was complete sample separation in two or more pieces. The number of cycles to failure covered by the tests is between  $10^3$  to  $10^7$  cycles.

### 3. STRESS ANALYSIS

The stress state in the V-notched specimen has been evaluated by structural analysis performed with the code ABAQUS 6.7, using a hybrid mesh composed by second order C3D10M tetrahedral elements and C3D20R hexahedral elements. After carrying out an analysis on the whole model, a finer resolution of the stress state around the notch tip was performed using the submodel technique. The global model is meshed with 34694 elements and the submodel is a  $10^\circ$  slice with 50570 elements, having the smallest element length of  $13 \mu\text{m}$ .

The material is implemented as transverse isotropic linear elastic, using the elastic constants estimated from off-axis tests on dog-boned specimens (thickness  $t = 3 \text{ mm}$ ) in a previous investigation [6] and reported in Table 1.

**Table 1:** Elastic constants used for structural simulation of the V-notched tubular specimen

$E_1$ [GPa]	$E_2$ [GPa]	$G_{12}$ [GPa]	$\nu_{12}$ [-]
8.55	7.10	2.56	0.40

1 represents fibre direction, 2 the circumferential direction, and 3 is the third material axes defined by 1 and 2 using the right hand rule. Fibres are assumed to be aligned in melt flow direction, along the specimen profile. Geometrical non-linearity is not activated in the simulation.

Under pure axial loading, the stress state around the notch tip results fully triaxial, as displayed in Figure 3, while under pure torsional loading only the shear component is relevant for the stress state in the material reference system (refer to Figure 1). For the same nominal load, the shear stress distribution  $\tau_{12}$  under pure torsional loading, along the specimen thickness, is flatter than the normal stress distribution  $\sigma_1$  under pure axial loading (Figure 4). Thus, the relative gradients of the stress distributions differ substantially from each other. The theoretical stress concentration factor obtained from FEA is  $K_t = \sigma_{p1,ep} / \sigma_{p1,nom} = \sigma_{1,ep} / \sigma_{1,nom} = 5.17$  for pure axial loading and  $K_{ts} = \tau_{12,ep} / \tau_{12,nom} = \sigma_{p1,ep} / \sigma_{p1,nom} = 2.44$  for pure torsional loading.

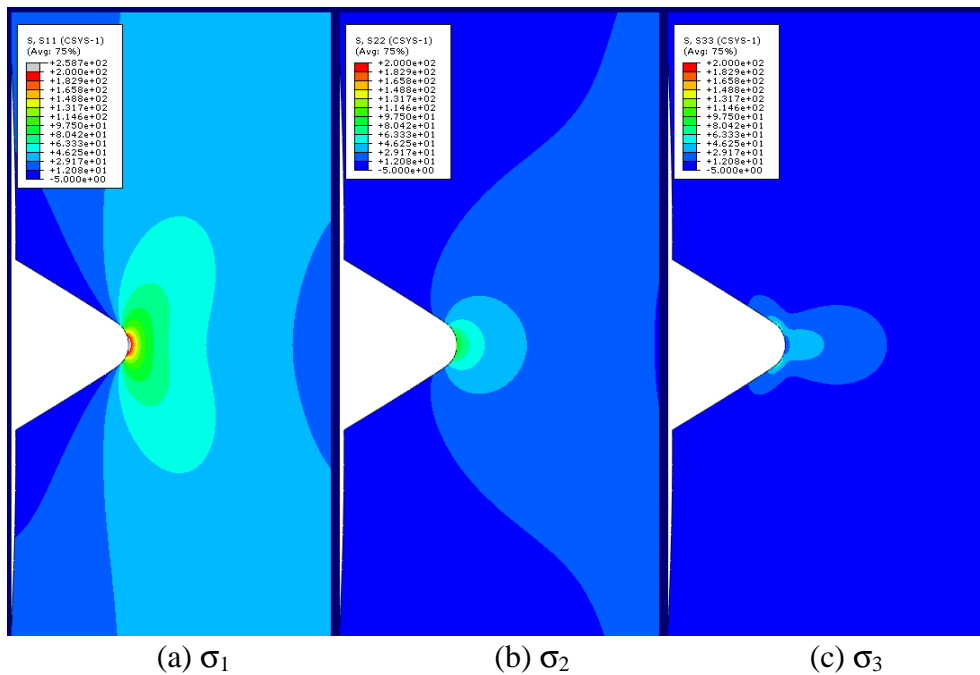


Figure 3: Stress contours in the material reference system under pure axial loading with  $\sigma_{x,nom} = 50$  MPa

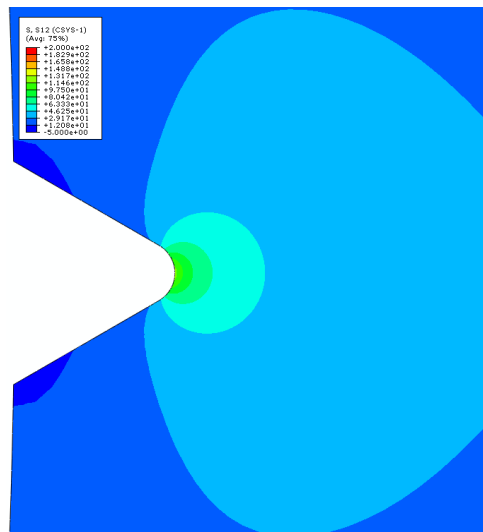


Figure 4: Shear stress contour in the material reference system under pure torsional loading with  $\tau_{xy,nom} = 50$  MPa

#### 4. DATA PRESENTATION

All fatigue data are analysed with the classical stress-life approach, drawing the data in terms of nominal stress amplitudes in the geometrical reference system  $\sigma_{x,a}$ ,  $\tau_{xy,a}$  versus the number of cycles to failure  $N$ . Stresses are computed referring to the net section; the nominal shear stress refers to the external surface of the specimen, according to the well-known Coulomb formulation:

$$\tau_{XY,nom} = \frac{M_t}{W_t} = \frac{M_t}{J_p} \cdot R_e \quad (1)$$

where  $M_t$  is the applied torque moment,  $W_t$  the section modulus and  $J_p$  the polar moment of inertia and  $R_e$  the external radius, referring to the median cross-section of the specimen. At this position, the fibres are mainly aligned along the specimen axis  $X$ , so that the stress components in the material and geometrical reference system are the same ( $\sigma_I = \sigma_x$  and  $\tau_{I2} = \tau_{xy}$ ).

Test results are reported in double logarithmic diagrams for  $R = 0$  and for  $R = -1$  in [Figure 5a](#) and [Figure 5b](#) respectively. Except for pure torsional loading, for which the nominal shear stress  $\tau_{I2}$  is used, all data are expressed in terms of nominal stress in fibre direction  $\sigma_I$ .

The following model formulation is used to interpolate the number of cycles to failure  $N$  as a function of the geometrical applied stresses  $\sigma_{i,a}(N)$ :

$$N = 10^6 \cdot \left( \frac{\sigma_{i,A}}{\sigma_{i,a}(N)} \right)^k \quad \sigma_{i,a}(N) = \sigma_{x,a}(N), \tau_{xy,a}(N) \quad (2)$$

where  $\sigma_{i,A}$  and  $k$  are two fitting parameters.  $\sigma_{i,A}$  represents the geometrical stress (refer to [Figure 1](#) for coordinate system definition) required to cause failure at  $N=10^6$  cycles, while  $k$  is the inverse slope of the fatigue curve. Details on the fitting procedure are reported in [4]. Errors on response are assumed to be normally distributed with constant variance. The fitting parameters for the different curves, together with their 95% confidence bands, and the scatter indexes  $T_\sigma$  (referring to the ratio, at the reference number of cycles  $N = 10^6$ , between the stress value at 90% and 10% failure probability) are summarised in [Table 1](#).

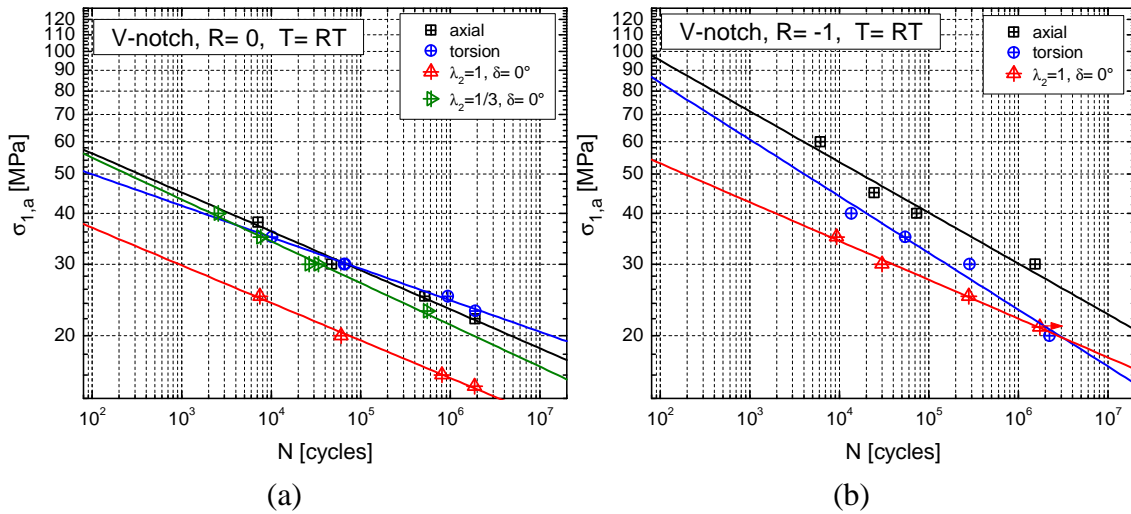


**Figure 5:** Fatigue curves for V-notched tubular specimens at RT for  $R = 0$  (a) and  $R = -1$  (b) in terms of nominal net stress amplitudes

**Table 1:** Summary of Wöhler parameters for the notched multiaxial fatigue tests

Series	T [°C]	R [-]	$\lambda_2$ [-]	$\delta$ [°]	$\sigma_{i,A}$ [MPa]	Conf. [MPa]	k [-]	Conf. [-]	$T_\sigma$ [-]
1	RT	0	0	-	23.21	+ 1.90 - 2.07	10.42	± 3.03	1.080
2	RT	-1	0	-	30.08	+ 5.61 - 6.89	8.00	± 3.02	1.211
3	RT	0	$\infty$	-	24.43*	+ 0.67 - 0.69	12.89	± 1.83	1.034
4	RT	-1	$\infty$	-	23.16*	+ 4.13 - 5.03	7.16	± 3.01	1.212
5	RT	0	1	0	15.72	+ 0.92 - 0.98	10.81	± 3.03	1.045
6	RT	-1	1	0	22.02	+ 1.65 - 1.79	10.47	± 3.03	1.059
7	RT	0	$\frac{1}{3}$	0	21.25	+ 1.57 - 1.69	9.72	± 1.83	1.091

\*In this field the value refers to torsional stress amplitude  $\tau_{12,a}$  at  $N=10^6$  cycles

Details for the fitting procedure, the calculation of  $T_\sigma$  and of the confidence intervals for the regression parameters are reported in [5] and [7]. Due to small number of fatigue data for each series, a Gaussian normal distribution was assumed for the scatter calculation, alternatively to the formula proposed by Natrella [8].

Figure 5 shows that the allowable nominal shear stress level under pure torsional loading is comparable to the nominal normal stress under pure axial loading. In view of such evidence, a combined load with  $\lambda_2 = 1/3$  is dominated by the axial load component, as confirmed by the superposition of the corresponding S-N curve with the pure axial one in Figure 5a; the series  $\lambda_2 = 1/3$  was therefore cancelled from the experimental program for  $R = -1$ . The slope of fatigue curves seems to be slightly influenced by the loading conditions; considering the 95% confidence bands on the slope parameters (see Table 1), however, this difference is not statistically significant.

Analysing the fracture patterns of the different series, two characteristic crack paths can be identified; they are reported in Figure 6. Pure axial loading ( $R = 0$  as well as  $R = -1$ ), combined loading with  $R = 0$ ,  $\lambda_2 = 1/3$  and  $R = -1$ ,  $\lambda_2 = 1$  and even pure torsional loading with  $R = -1$  present the fracture pattern of Figure 6a: crack nucleates and propagates along the circumferential direction as well as through the thickness, until specimen separation occurs. In the case of axial loading, propagation occurs via mode I, while for torsional loading it is via mode II; for the combined cases, a combination of both modes takes place. Pure torsion with  $R = 0$  and combined loading with  $R = 0$ ,  $\lambda_2 = 1$ , display the crack path of Figure 6b: crack first propagates through the thickness, then along the circumferential direction and eventually along a plane of  $45^\circ$  from axial direction X. A switch between the two propagation mechanisms is presumably induced by frictional forces between fracture surfaces. Such transition does not occur for torsional loading with  $R = -1$  because the alternating load causes abrasion between the crack surfaces, which substantially reduces the frictional forces, avoiding the activation of crack propagation along the  $45^\circ$  plane. Crack onset usually occurs next to the mould dividing line on injection side, where fibres alignment in flow direction is not pronounced and a significant *core layer* is encountered (compare Figure 9 and Figure 10): this zone represents the weakest region of the medial cross-section of the specimen.

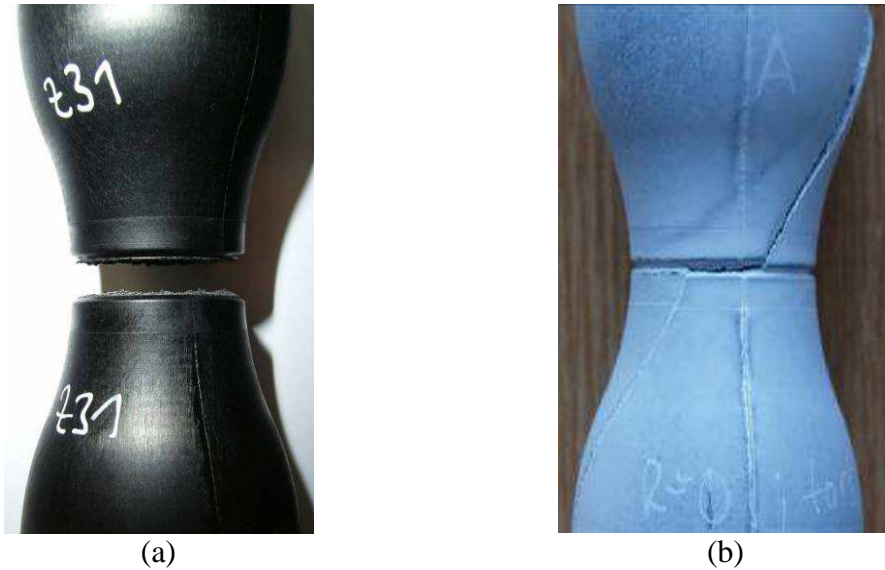


**Figure 6:** Representative fracture patterns for V-notched tubular specimens

## 5. COMPARISON TO PLAIN SPECIMENS

As a first analysis, the nominal S-N curves of the V-notched specimens are compared to the relevant curves of plain tubular specimens reported in [5], in order to analyse the notch effect on fatigue strength. Figure 7a and Figure 7b show the notch influence under uniaxial loading for  $R=0$  and  $R=-1$  respectively. As usual, normal stress in fibre direction  $\sigma_l$  is reported for axial loading and shear stress  $\tau_{l2}$  is adopted for torsional loading.

Compared to the plain specimens, the V-notch affects remarkably the fatigue behaviour under pure axial loading, causing a fatigue strength reduction on  $\sigma_{l,A}$  of 48% for  $R = 0$  and 53% for  $R = -1$ . As regards pure torsional loading, almost no strength reduction can be observed, in terms of nominal shear stress, for  $R = 0$  as well as for  $R = -1$ . This result is quite surprising and details will be further discussed in the next section.

Figure 8 presents the notch effect under combined loading conditions, comparing the plain and V-notched fatigue curves.

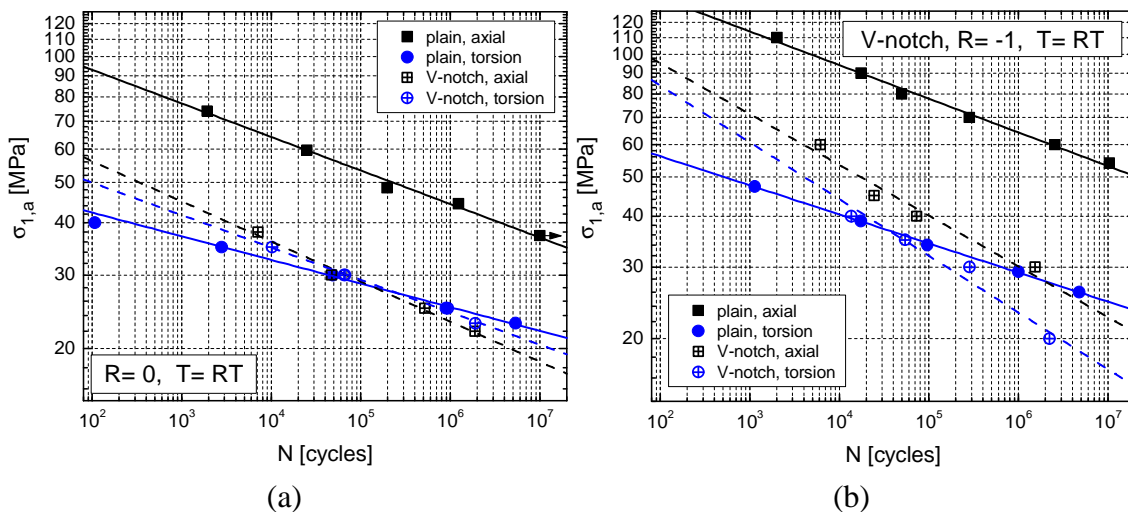


**Figure 7:** Comparison between fatigue curves of plain and V-notched tubular specimens at RT under pure loading conditions with  $R = 0$  (a)  $R = -1$  (b)

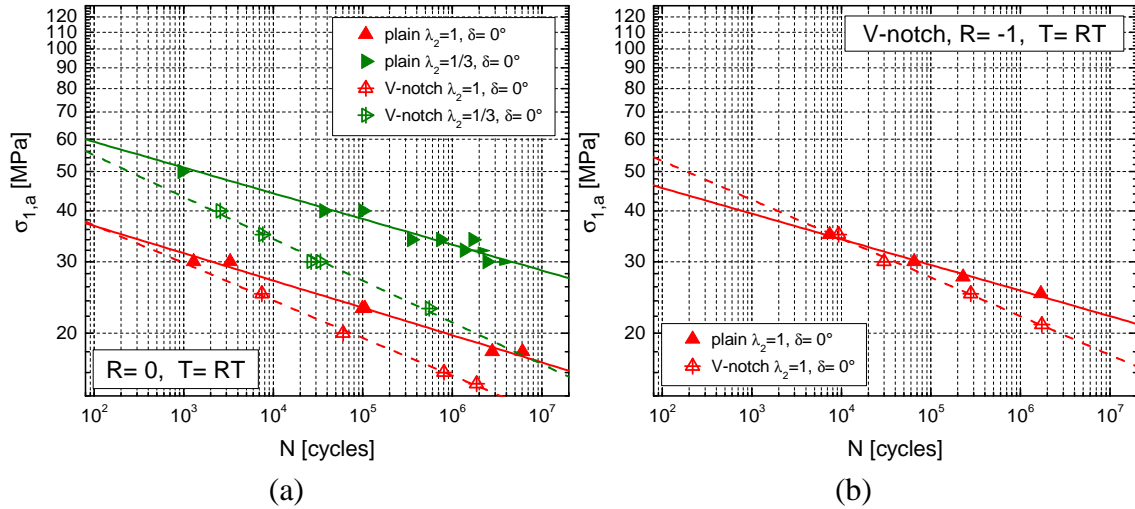


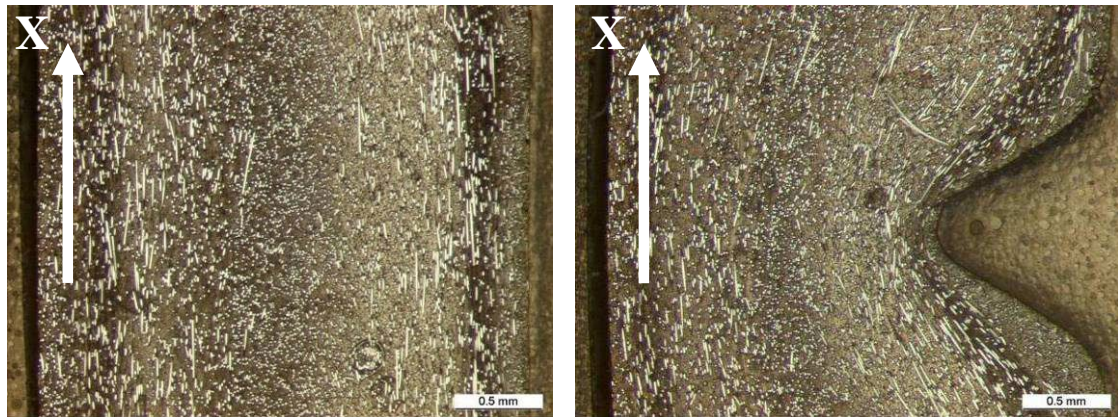
**Figure 8:** Comparison between fatigue curves of plain and V-notched tubular specimens at RT under combined loading conditions with  $R = 0$  (a)  $R = -1$  (b)

For  $R = 0$ , the notch induces a strength decrease, which is larger for smaller  $\lambda_2$ ; for  $R = -1$  the strength reduction is evident only at cycles to failure  $N$  larger than  $10^5$ . Presumably, for the same biaxiality ratio, the torsional component has a bigger influence for  $R = -1$  than it has for  $R = 0$ . Figure 7 and Figure 8 show that S-N curves for V-notched specimens are steeper (lower  $k$  value) than those of plain specimens. The notch thus affects not only the fatigue strength level but also the fatigue slope.

## 6. NOTCH-EFFECT UNDER TORSIONAL LOADING

Under pure torsional loading, the fatigue curves of the almost plain and the V-notched tubular specimens are superposed, for  $R = 0$  as well as for  $R = -1$ ; apparently, no notch-sensitivity is recorded under this loading condition. It is questionable whether such result is due to intrinsic material properties or to geometrical and/or morphological considerations. Indeed, the specimen thickness in the medial cross-section, is  $t = 2$  mm for the V-notched specimen, against  $t = 3$  mm of the plain tubular specimen. This difference induces different morphological configurations: in the medial cross-section of the specimen, the fibre orientation (FO) distribution of the V-notched specimen is expected to be more pronounced than in the almost plain specimen, due to the smaller thickness and to the section restriction, which induces a steeper velocity profile of the polymer melt along the thickness. In order to compare the morphological configurations of the two specimens, they were cut along the X-Y plane (refer to Figure 1), defined by the two mould dividing lines. In order to increase the contrast between fibres and matrix, the samples were pre-treated by oxygen plasma etching for 40 minutes. The obtained sections are reported in Figure 9 and Figure 10 for the mould dividing line, on injection side and opposite to injection side respectively. The latter is representative of the morphological configuration of a generic section passing through an arbitrary radial direction.

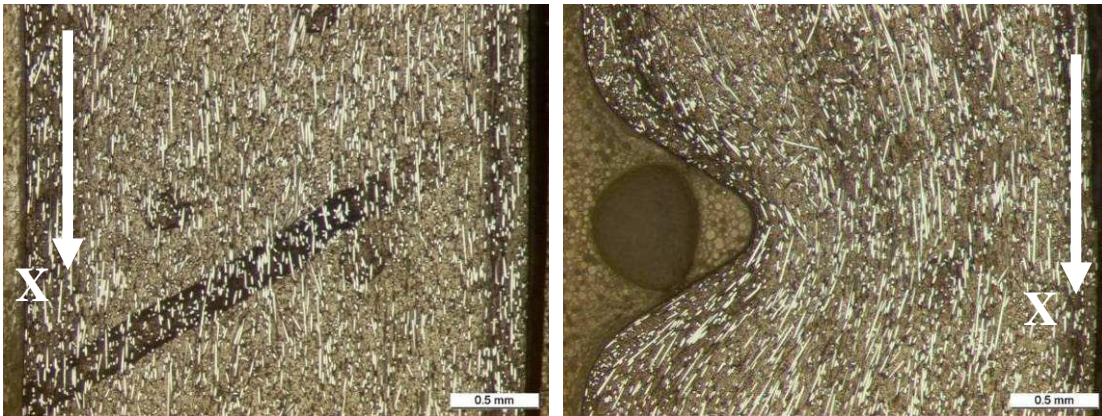
The darker strip in Figure 10a results from the etching process and could not be removed by a non-abrasive cleaning process. From the reported pictures, no pronounced morphological differences are evident on injection side, while a slightly better fibre alignment in X direction can be noticed opposite to injection side.



(a) Plain

(b) Notched

**Figure 9:** Comparison of a longitudinal section of the plain (a) and V-notched (b) tubular specimens along the mould dividing line on injection side



(a) Plain

(b) Notched

**Figure 10:** Comparison of a longitudinal section of the plain (a) and V-notched (b) tubular specimens along the mould dividing line opposite to injection side

No core layer appears in [Figure 10a](#) as well as [Figure 10b](#). As a further consideration, the notch geometry induces a thickness variation along the cross-section, so that the absolute radial distance, at which the nominal stress is calculated, is not the same for the two specimens. [Figure 11](#) compares the shear stress distributions from FEA for the same nominal applied load. The outer surface of the V-notched specimen is situated at  $t = 0$  mm, while that of plain specimen lays at  $t = -1$  mm, arising some doubts in the comparison. Another difference between the notched and plain fatigue series concerns the failure modes: for the plain specimen, crack initiates on a longitudinal plane, parallel to nominal fibre direction, while for the notched specimen, crack onset is along a transversal plane, perpendicular to fibre direction. Some representative failure pictures are reported in [Figure 13](#). The shear strength in the transversal plane  $\tau_{12,u}$  is presumably higher than the strength of the longitudinal plane  $\tau_{21,u}$ , due to different material reinforcement induced by the fibres. Reasonably, there is compensation between the notch-effect, which causes a strength reduction, and the failure-mode-effect, which is responsible for a larger shear strength value on the transversal plane, compared to the longitudinal one. In order to clarify the reasons of the apparent notch insensitivity, the authors decided to carry out a further test series on a different notch geometry, namely a drilled circular hole of radius  $\rho = 1$  mm. To grant the same morphology in the notched and plain specimen, the notch was shaped by machining of plain specimens.

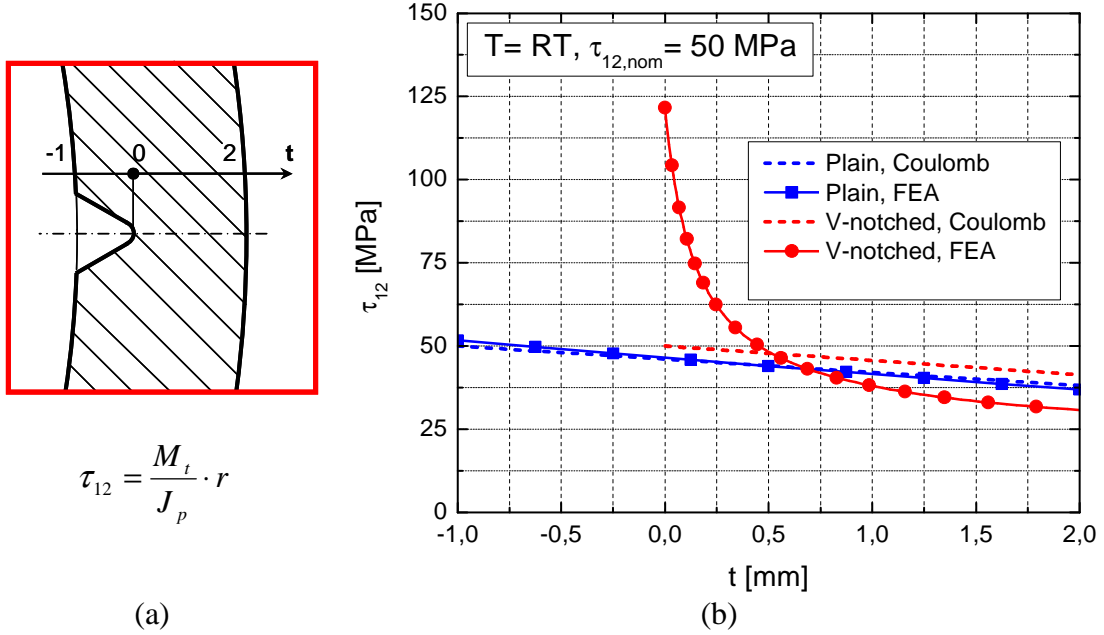


**Figure 11:** Comparison between shear stress distribution along the thickness for plain and V-notched tubular specimens

The holes were carefully drilled in the central part of the plain tubular specimen at a circumferential angle of  $90^\circ$  from the radial direction corresponding to the mould dividing lines. The nominal shear stress on the drilled specimen is computed with equation (1), using following formula to calculate the polar moment:

$$J_p = \int_A r^2 dA = \int_{R_i}^{R_e} r^2 \cdot 2 \left[ \pi - \arctg\left(\frac{\rho}{r}\right) \right] r \cdot dr \quad (3)$$

$R_i$  and  $R_e$  are the internal and external radius of the tubular specimen respectively, while  $r$  is the radial integration coordinate. For thin cylindrical specimens, the hole walls can be assumed to have radial direction, leading to an approximate formulation of (3):

$$J_p = \int_{R_i}^{R_e} r^2 \cdot 2 (\pi - \gamma) r \cdot dr = \frac{\pi - \gamma}{2} (R_e^4 - R_i^4) \quad (4)$$

where  $2\gamma$  is the angle formed by the radial axes delimiting the hole on the cross-section of the specimen. Equation (4) slightly overestimates  $J_p$ , but the error is certainly negligible from an engineering point of view. For the considered geometry it is  $W_t = 1959.89 \text{ mm}^3$ . A preliminar structural simulation delivered a shear stress concentration factor  $K_{ts} = \tau_{12, ep} / \tau_{12, nom}$  of 2.12.

The S-N curve under pure torsion for the drilled specimen is displayed in Figure 12, in comparison with the analogous curves of the plain and V-notched tubular specimens. Interestingly, this time a fatigue strength reduction on  $\tau_{12, A}$  of 35% is recorded. This value is not as high as the one obtained for the V-notch under pure axial loading but it is anyway a considerable decrease, also considering that the two notch radii are quite different. Moreover the S-N curve for the specimen with hole appears steeper than the one for plain specimen. However, it is important to underline that the notch machining damages the surface of the specimen, probably facilitating crack onset at the surface.

Figure 13 displays a comparison of characteristic fracture lines for the three considered specimens.

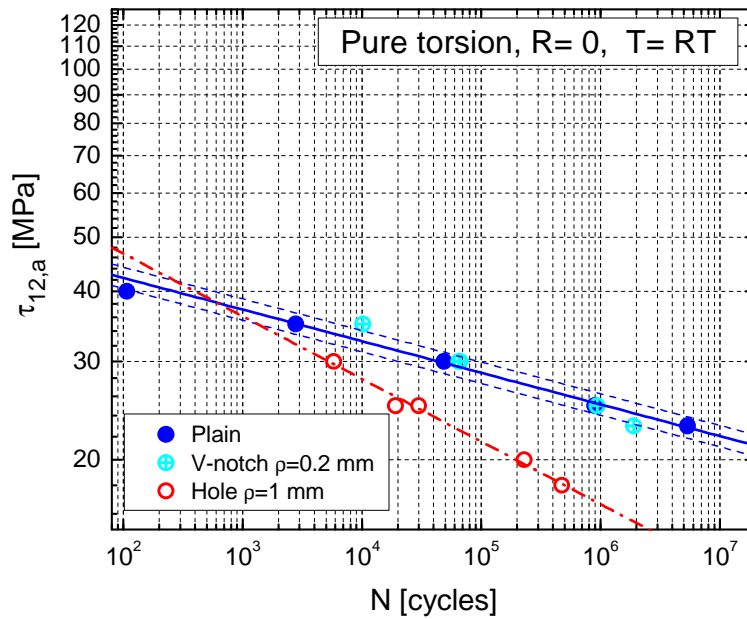


**Figure 12:** Comparison of fatigue curves for plain, V-notched and holed tubular specimens under pure torsional loading with  $R=0$  at RT

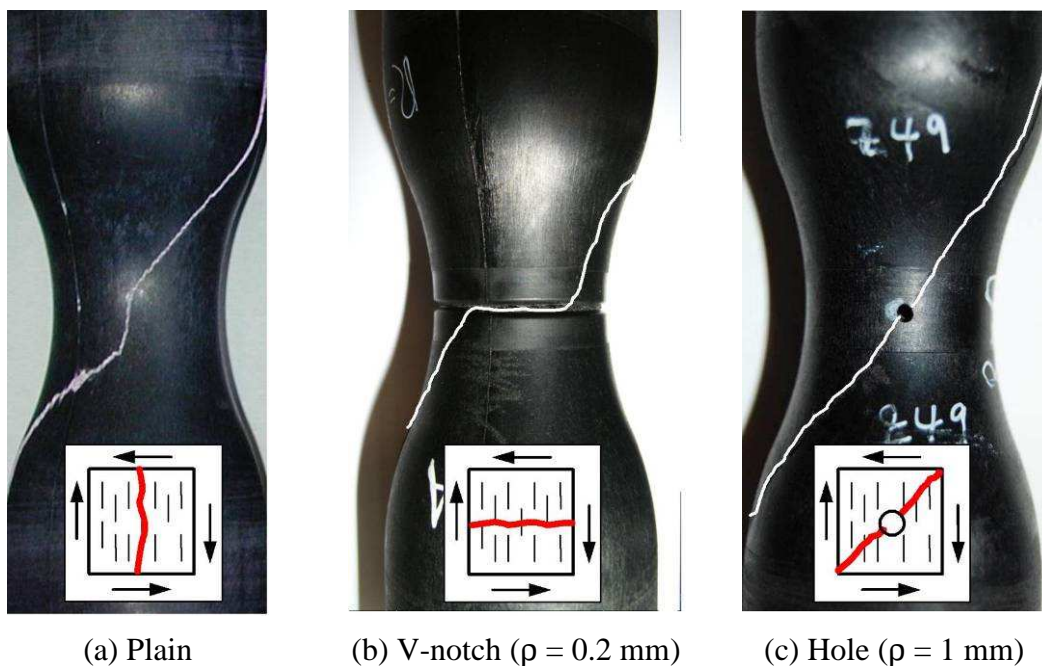


**Figure 13:** Comparison of typical failure modes for plain (a), V-notched (b) and holed (c) tubular specimens under pure torsional loading with  $R=0$  at RT

For the specimen with hole, the crack onset location and propagation path recalls the failure pattern of an isotropic material, where crack propagation is determined by the first principal stress  $\sigma_{p1}$ . Different failure modes occur for each of the curves plotted in Figure 12. For the plain and the V-notched specimen crack is initiated via mode II, along the longitudinal and transversal maximum shear planes respectively. A correlation of the S-N curves to failure modes require further investigations.

In conclusion, the results on specimens with hole show that the material is notch sensitive under cyclic shear stresses. The superposition of S-N curves for the plain and V-notched specimens is believed to be the result of compensation between the effect of stress concentration introduced by the notch and effects involving morphology,

geometry and failure modes. A decoupling of these effects would be desirable for the comprehensive understanding of the fatigue behaviour. However, the feasibility of a suitable specimen is restricted by the conditions imposed by the manufacturing process. Ignoring the different failure modes and morphology between the V-notched and plain tubular specimens, a modelling of the data with empirical criteria will be anyway attempted in a following contribution.

## 7. CONCLUSIONS

The multiaxial fatigue behaviour of V-notched hollow tubular specimens, made of PA66-GF35, was investigated, extending the characterisation on plain tubular specimens presented in [5]. Contrary to plain specimens, the allowable nominal shear and axial stress under the respective uniaxial loading cases were comparable. However, the stress concentration introduced by the notch under axial loading is larger than the one under torsional loading. Compared to plain specimens, steeper fatigue curves were observed for the notched specimens. A considerable strength reduction was displayed by the fatigue curves under pure axial loading, whereas fatigue curves of V-notched and plain specimens under pure torsional loading are superimposed. The failure modes, the morphological configuration of the medial cross-section and the radial position of the elastic peak shear stress were however different. A further torsional fatigue curve on a tubular specimen containing a drilled hole displayed lower fatigue strength, revealing a notch-sensitivity of the material even for shear stresses.

## REFERENCES

1. Francis P.H., Walrath D.E., Sims D.F., Weed D.N., "Biaxial fatigue loading of notched composites", *Journal of Composite Materials* 1977; 11: 488-501
2. Fujii T., Shiina T., Okubo K., "Fatigue notch sensitivity of glass woven fabric composite having a circular hole under tension/torsion biaxial loading", *Journal of Composite Materials* 1994; 28(3): 234-251
3. Sonsino C.M., Moosbrugger E., "Fatigue design of high loaded short-glass-fibre reinforced polyamide parts in engine compartments", *Int. J. Fatigue* 2008; 30: 1279-1288
4. De Monte M., Quaresimin M., Lazzarin P., "Modelling of fatigue strength data for a short fibre reinforced polyamide 6.6 based on local strain energy density", *Proceedings of the 16<sup>th</sup> International Conference on Composite Materials*, Ed. Japan Society for Composite Materials, 8-13 July 2007, Kyoto, Japan
5. De Monte M., Moosbrugger E., Jaschek K., Quaresimin M., "Multiaxial fatigue of a short glass fibre reinforced polyamide 6.6 – Fatigue and fracture behaviour", accepted for publication on *Int. J. Fatigue*
6. De Monte M., Moosbrugger E., Quaresimin M., "Influence of temperature and thickness on the off-axis behaviour of short glass fibre reinforced polyamide 6.6 – Quasi-static loading", to appear
7. De Monte M., Moosbrugger E., Quaresimin M., "Influence of temperature and thickness on the off-axis behaviour of short glass fibre reinforced polyamide 6.6 – Cyclic loading", to appear
8. Natrella M.G., *Experimental statistics, Handbook 91*, National Bureau of Standards; 1966, pp. 2-15